**Geomechanics and Engineering**, *Vol. 7, No. 6 (2014) 679-703*
DOI: http://dx.doi.org/10.12989/gae.2014.7.6.679


# Nonlinear response of laterally loaded rigid piles in sand

Hongyu Qin [*1] and Wei Dong Guo [2]

[1] *School of Computer Science, Engineering and Mathematics, Flinders University, Adelaide, SA 5001, Australia*
[2] *School of Civil, Mining and Environmental Engineering, University of Wollongong, NSW 2522, Australia*

(*Received October 14, 2013, Revised July 27, 2014, Accepted August 21, 2014*)

**Abstract.** This paper investigates nonlinear response of 51 laterally loaded rigid piles in sand. Measured response of each pile test was used to deduce input parameters of modulus of subgrade reaction and the gradient of the linear limiting force profile using elastic-plastic solutions. Normalised load - displacement and/or moment - rotation curves and in some cases bending moment and displacement distributions with depth are provided for all the pile tests, to show the effect of load eccentricity on the nonlinear pile response and pile capacity. The values of modulus of subgrade reaction and the gradient of the linear limiting force profile may be used in the design of laterally loaded rigid piles in sand.

**Keywords:** piles; lateral loading; shear modulus; modulus of subgrade reaction; ultimate soil resistance

## 1. Introduction

Extensive theoretical studies, in-situ full-scale tests and laboratory model tests have been carried out on laterally loaded rigid piles in cohesionless soils (Poulos and Davis 1980, Scott 1981, Dickin and Nazir 1999, Laman *et al.*1999, Guo 2008, Zhang *et al.* 2005, Zhang 2009, Chen *et al.* 2011). Several methods have been developed for predicting lateral capacity of rigid piles based on an assumed profile of soil resistance per unit length along a pile (Brinch Hansen 1961, Broms 1964, Petrasovits and Awad 1972, Meyerhof *et al*. 1981, Fleming *et al*. 2009, Prasad and Chari 1999). The capacity was also determined as the load at a certain displacement from a measured lateral load- displacement or the moment with reference to a specified pile rotation angle from a measured moment - rotation curve (Broms 1964, Haldar *et al*. 2000, Chen *et al.* 2011). These methods, nevertheless offer different lateral capacities for same measured data. To resolve the issue, Guo (2008) established elastic-plastic solutions for analysing laterally loaded rigid piles, assuming a constant modulus of subgrade reaction or a linearly increasing modulus of subgrade reaction with depth together with a linear limiting force profile (LFP). Presented in explicit expressions in terms of the slip depths mobilised from the ground line and pile tip, the solutions enable nonlinear response of piles and displacement-based capacity to be estimated. The estimations are satisfactory against the pile responses in model tests presented by Prasad and Chari (1999) and the experimental and numerical analysis results by Laman *et al.* (1999).

*Corresponding author, Ph.D., E-mail: hongyuqin@gmail.com

Significant research effort has also been made to study passive piles subjected to lateral soil movements based on field monitoring and analysis, centrifuge and laboratory model tests, analytical and numerical analysis as reviewed by Qin (2010). The study indicates the analysis of the piles requires the modulus of subgrade reaction or Young's modulus of the soil and limiting force $p_u$ profile (Poulos *et al*. 1995, Guo 2006, 2013a), which may be related to those for laterally loaded piles discussed herein (Guo 2013b).

In this paper, elastic-plastic solutions were used to study the measured response of 51 laterally loaded pile tests in sand, including 16 full-scale field tests, 12 centrifuge tests and 23 laboratory model tests. This is illustrated in light of a full-scale field test to demonstrate the calculation and its reliability. The study examines the impact of load eccentricity on the nonlinear pile response, range of modulus of subgrade reaction, average shear modulus and limiting force profile for laterally loaded rigid piles in sand.

## 2. Elastic-plastic solutions

A free-headed pile with a lateral load $T_t$ applied at an eccentricity $e$ above the groundline is schematically shown in Fig. 1(a). The pile is defined as rigid if the pile-soil relative stiffness, $E_P/G_s$ exceeds a critical ratio $(E_P/G_s)_c$, where $(E_P/G_s)_c$= $0.052(l/r_0)^4$ (Guo and Lee 2001), $E_P$ is the effective Young's modulus, defined as $E_P$= $(EI)_P/(\pi r_0^4/4)$, $(EI)_P$is thepile bending rigidity, $G_s$ is the shear modulus of the soil, $l$ is the pile embedded length and $r_0$ is the outer radius of the pile.

### *2.1 Load transfer model*

Guo (2008) provides a pile-soil interaction model characterised by a series of springs distributed along the shaft. Each spring has an idealised elastic-plastic *p*-*y*(*u*) curve at any depth shown in Fig. 1(b). The soil resistance per unit length $p$ is proportional to the local displacement $u$ at that depth and to the modulus of subgrade reaction $kd$ by

$$p = kdu \quad \text{(Elastic state)} \tag{1}$$

The magnitude of $k$ is related to the average shear modulus $\overline{G}_s$ by

$$kd = \frac{3\pi\overline{G}_s}{2}\left\{2\gamma\frac{K_1(\gamma)}{K_0(\gamma)} - \gamma^2\left[\left(\frac{K_1(\gamma)}{K_0(\gamma)}\right)^2 - 1\right]\right\} \tag{2}$$

where $d$ is the outer diameter of the pile, $\overline{G}_s$ is an average shear modulus of the soil over the pile embedded length, $K_i(\gamma)$ is the modified Bessel function of second kind of $i^{\text{th}}$ order ($i$ = 0,1), $\gamma$ is a non-dimensional factor given by $\gamma = k_1r_0/l$, , $k_1$ = 2.14 and 3.8 for pure lateral load ($e$ = 0) and pure moment loading ($e = \infty$), respectively. The value of $k_1$ can be approximately estimated by $k_1$ = 2.14 + $e/l/(0.2+0.6e/l)$, increasing from 2.14 to 3.8 as $e$ increase from 0 to $\infty$ (Guo 2012). The $k$ may be written as $k_0z^m$ [$k_0$, $FL^{-m-3}$], with $m$ = 0 and 1 being referred to as constant $k$ ($k = k_0$) and Gibson $k$ ($k = k_0z$) hereafter. For the constant $k$ and Gibson $k$, the $k$ and $k_0$ have a unit of MN/m$^3$ and MN/m$^4$, respectively.

Once the local pile displacement u exceeds a threshold value of $u$* as seen in Fig. 1(b), $p$

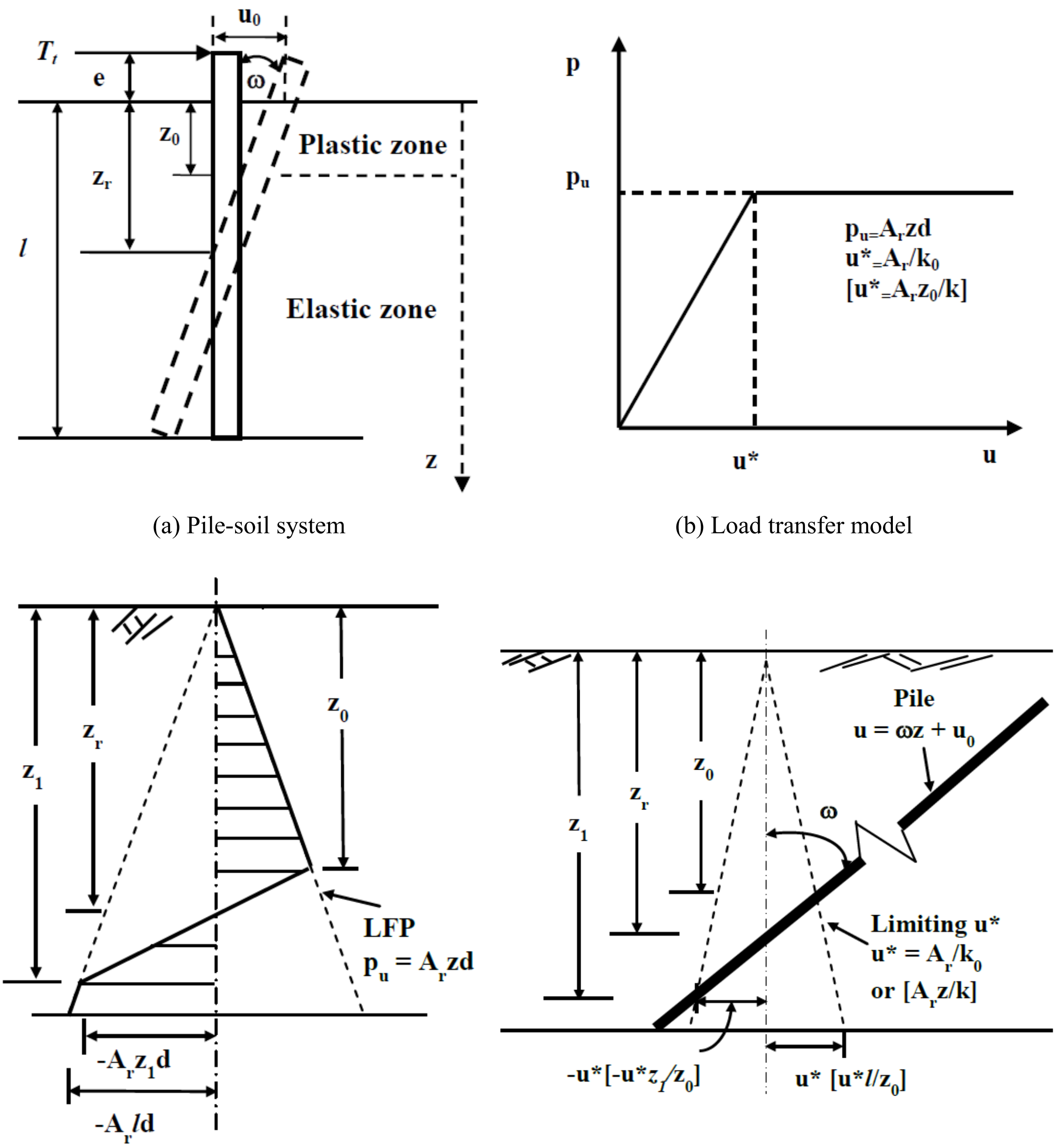


(a) Pile-soil system (b) Load transfer model

(c) $p_u$ profile (d) Pile deflection features

$e$ = loading eccentricity above ground line; $T_t$ = lateral load; $u_0$= pile displacement at ground line; angle of rotation (in radian); $z$ = depth from ground line; $l$ = embedded length; $z_0$ = depth of slip; $z_r$ = depth of rotation point; $p$ = soil resistance per unit length; $p_u$= ultimate soil resistance per unit length; $A_r$ = gradient of limiting force profile; $d$ = outer diameter of the pile; $u$ = pile displacement; $u^*$ = local threshold u above which pile soil relative slip is initiated; $k$, $k_0$ = modulus of subgrade reaction, $k = k_0z^m$, $m$ = 0, and 1 for constant and Gibson $k$.

Fig. 1 Schematic analysis for a rigid pile (after Guo 2008) the limiting value $p_u$ and the pile-soil relative slip is initiated. It is assumed that the $p_u$ increases linearly with depth $z$ as shown by the dashed line in Fig. 1(c) and may be described by

$$p_u = A_r z d \quad \text{(Plastic state)} \tag{3}$$

where $A_r z$ is the net limiting pressure on the pile surface and $A_r$ may be expressed as

$$A_r = N_g \gamma'_s K_p^2 \tag{4}$$

where $\gamma'_s$ is the effective unit weight of the soil, i.e., bulk unit weight above water table and buoyant unit weight below, $K_p = \tan^2 (45° + \varphi'_s/2)$ is the coefficient of passive earth pressure, $\varphi'_s$ is an effective frictional angle of the soil, $N_g$ is a non-dimensional parameter. The actual $N_g$ can be back- calculated from the measured pile responses as shown later.

### *2.2 Explicit expressions for the solutions*

Typical pile-soil interaction states and pile displacement modes have been defined as follows.The pile has a displacement $u = \omega z + u_0$. It rotates about a depth $z_r$ (= $-u_0/\omega$) at which deflection $u = 0$, note $u_0$ is the pile displacement at ground line, $\omega$ is the rotational angle in Fig. 1(d). The soil resistance per unit length $p$ attains the limiting force per unit length $p_u$ once the deflection $u$ exceeds $u^*$ [= $A_r/k_0$ (Gibson $k$) or = $A_r z_0/k$ (constant $k$)]. The soil resistance $p$ along the pile, i.e., the on-pile force distribution is illustrated in Fig. 1(c).The on-pile force per unit length $p$ follows the positive $p_u$ profile given by Eq. (3) to a slip depth $z_0$ from groundline. In other words, the pile soil interaction is in plastic state. Below the $z_0$, it is described by Eq. (1) since the pile-soil interaction is still in elastic state. In particular, once the pile tip-displacement $u$ ($z = l$) touches $-u^*$ (Gibson $k$) or $-u^* l/z_0$ (constant $k$), or the soil resistance $p$ ($z = l$) at the pile-tip touches $A_r ld$, the pile is said at *tip-yield state*. After the pile-tip yields, increasing loading will also result in pile-soil relative slip initiating from the pile-tip and expanding upwards to another slip depth$z_1$ as illustrated in Fig. 1(c). The two plastic zones will merge eventually and the pile reaches the ultimate state, i.e., *yield at rotation* point ($z_0 = z_1 = z_r$).

The solutions are presented in explicit expressions characterized by the slip depths. Their non-dimensional forms for pre-tip yield and tip yield states are presented in Table 1 in form of normalised lateral load $T_t/(A_r dl^2)$, groundline displacement $u_0 k_0/A_r$ (Gibson $k$) or $u_0 k/(lA_r)$ (constant $k$), rotation angle $\omega k_0 l/A_r$ (Gibson $k$) or $\omega k/A_r$ (constant $k$), depth of maximum bending moment $z_m$, and maximum bending moment $M_{\max}/(A_r dl^3)$. The reader is referred to Guo (2008) for details of the solutions.

The solutions were entered into a spreadsheet program, which adopts user-defined macros in Microsoft Excel VBA. The input parameters are as follows: (1) pile dimensions $d$ and $l$, and soil parameters $\varphi'_s$ and $\gamma'_s$, (2) loading eccentricity $e$, and (3) parameters $A_r$ and $k$ (or $k_0$).Given a set of input parameters, nonlinear response and ultimate lateral capacity of the pile can be predicted. Conversely, the parameters $A_r$ and $k$ (or $k_0$) may be deduced from measured responses of laterally loaded piles using the closed-form solutions.

## 3. Analysis of measured pile responses

51 pile tests in horizontal ground were studied, comprising 16 full-scale field tests, 12 centrifuge

Table 1 Solutions for pre-tip and tip yield state (Guo 2008)

| $u = \omega z + u_0$ and $z_r/l = -u_0/\omega l$ | |
|---|---|
| $p = kdu$, $p_u = A_r dz$, $kd$ is the modulus of subgrade reaction, $k$ is written as $k_0 z^m$. | |
| Gibson $k$ ($m$ = 1) | Constant $k$ ($m$ = 0) |
| $\frac{T_t}{A_r dl^2} = \frac{1}{6}\frac{1+2\bar{z}_0+3\bar{z}_0^2}{(2+\bar{z}_0)(2\bar{e}+\bar{z}_0)+3}$ | $\frac{T_t}{A_r dl^2} = \frac{\bar{z}_0}{2(2+3\bar{e}+\bar{z}_0)}$ |
| $\frac{u_0 k_0}{A_r} = \frac{3+2(2+\bar{z}_0^3)\bar{e}+\bar{z}_0^4}{[(2+\bar{z}_0)(2\bar{e}+\bar{z}_0)+3](1-\bar{z}_0)^2}$ | $\frac{u_0 k}{A_r l} = \frac{(2+3\bar{e})\bar{z}_0}{(2+3\bar{e}+\bar{z}_0)(1-\bar{z}_0)^2}$ |
| $\omega\frac{k_0 l}{A_r} = \frac{-2(2+3\bar{e})}{[(2+\bar{z}_0)(2\bar{e}+\bar{z}_0)+3](1-\bar{z}_0)^2}$ | $\omega\frac{k}{A_r} = \bar{z}_0\frac{\bar{z}_0^2+3(\bar{z}_0-2)\bar{e}-3}{[2+3\bar{e}+\bar{z}_0](1-\bar{z}_0)^2}$ |
| $\bar{z}_m = \sqrt{2T_t/(A_r dl^2)}\quad (z_m \le z_0)$ | $\bar{z}_m = \sqrt{2T_t/(A_r dl^2)}\quad (z_m \le z_0)$ |
| $M_{\max} = (2z_m/3+e)T_t\quad (z_m \le z_0)$ | $M_{\max} = (2z_m/3+e)T_t\quad (z_m \le z_0)$ |
| $(\bar{z}_0^y)^3+(2\bar{e}+1)(\bar{z}_0^y)^2+(2\bar{e}+1)\bar{z}_0^y-(\bar{e}+1)=0$ (Solving numerically) | $\bar{z}_0^y = -(1.5\bar{e}+0.5)+0.5\sqrt{5+12\bar{e}+9\bar{e}^2}$ |

*Note: $T_t$, $u$, $u_0$, $\omega$, $z$, $z_0$, $z_r$, $e$ and $l$ are defined in Fig. 1. $z_m$ is the depth of maximum bending moment $M_{\max}$, $z_0^y$ is the slip depth $z_0$ at tip yield state. $\bar{z}_0 = z_0/l$, $\bar{z}_m = z_m/l$, $\bar{e} = e/l$, $\bar{z}_0^y = z_0^y/l$.

tests and 23 model tests. The pile diameter $d$, embedded length $l$ and loading eccentricity $e$ are summarised in Table 2. The properties of sand including the relative density $D_r$, the angle of internal friction $\phi'_s$ and effective unit weight $\gamma'_s$ are presented in Table 3.The measured pile responses for selected tests are plotted as symbols in Figs. 2-9.

### *3.1 Back calculation*

Back calculations were carried out by best matching (via visual comparison) between the elastic-plastic solutions and the measured responses of the 51 test piles. This is sufficiently accurate as shown by the sensitivity analysis by Qin (2010). Theoretically, two measured load-displacement $T_t - u_0(u_t)$ and moment-rotation $M_0 - \omega$ curves are required to uniquely deduce the two parameters $A_r$ and $k$ (or $k_0$). With only one measured curve, either $T_t - u_0(u_t)$ or $M_0 - \omega$, back calculations were still carried out by fitting the initial elastic portion through adjusting $k$ (or $k_0$), and the last nonlinear portion of the curve by adjusting the $A_r$, as discussed later.

The deduced parameters $A_r$, $k_0$ and $k$ for each pile are presented in Table 3. Furthermore, the statistical analysis of the pile characteristics, soil properties and analysis results is presented in Qin (2010). The calculated pile responses with a Gibson $k$ and constant $k$ were plotted in Figs. 2-9 as dotted and solid lines, respectively, and as hollow dot points ○ and solid dots ● for those at tip-yield. This is illustrated next for the field test F1.

### *3.2 An example calculation – Field tests of steel pole foundations in loose sand*

Haldar *et al*. (2000) conducted eight full-scale field tests on fully instrumented steel trans-

Table 2 Characteristics of pile tests

| Test No. | Reference | Pile No. in reference | Pile type | $e$ (m) | $l$ (m) | $d$ (m) | Measured $M_u$ or $T_u$ | Measured curves |
|---|---|---|---|---|---|---|---|---|
| | | | **Full-scale field tests** | | | | | |
| F1 | Haldar *et al.* (2000) | 4 | Steel 12-sided steel polygonal pole | 22.25 | 3.20 | 0.755 | 855 kNm | $M_0 - \omega$, $M(z)$, $u(z)$ |
| F2 | | 1 | | 22.93 | 2.52 | 0.760 | 137 kNm | $M_0$ - $\omega$ |
| F3 | | 2 | | 22.94 | 2.52 | 0.760 | 253 kNm | |
| F4 | | 2A | | 22.86 | 2.59 | 0.761 | 615 kNm | |
| F5 | | 3 | | 22.86 | 2.59 | 0.759 | 726 kNm | |
| F6 | | 5 | | 22.88 | 2.57 | 0.759 | 654 kNm | |
| F7 | | 7 | | 22.86 | 2.59 | 0.759 | 674 kNm | |
| F8 | Bhushan *et al.* (1981) | 4 | Cast-in-place drilled piers | 0 | 5.50 | 0.610 | | $T$ - $u_0$ |
| F9 | | 5 | | 0 | 5.50 | 0.915 | | |
| F10 | | 6 | | 0 | 5.50 | 0.915 | | |
| F11 | | 7 | | 0 | 5.50 | 1.220 | | |
| F12 | Ismael and Klym(1981) | Footing 1 | Cased Augered pile | 0 | 6.40 | 0.9144 | 530 kN | $T$ - $u_0$, $M(z)$, $u(z)$ |
| F13 | Pender and Matuschka (1988) | Field test | Bored piers | 5.4 | 1.97 | 0.750 | 21.8 kN | $T$-$u_t$, $T$- $\omega$ |
| F14 | Lee *et al.* (2010) | T1 | Bored piles | 2.0 | 1.20 | 0.40 | 22 kN | $T$ - $u_0$ |
| F15 | | T2 | | 2.0 | 2.40 | 0.40 | 50 kN | |
| F16 | | T3 | | 0.15 | 2.40 | 0.40 | 210 kN | |
| | | | **Centrifuge tests** | | | | | |
| C1 | Georgiadis*et al.* (1992) | P1 | Stainless steel pipe pile | 1.25 | 9.05 | 1.092 | | $M(z)$, $T(z)$, $u(z)$ |
| C2 | | P2 | | 1.25 | 9.05 | 1.224 | | $T$- $u_t$, $M(z)$, $T(z)$, $u(z)$ |
| C3 | Laman*et al.* (1999) | 1 | Circular pier | 6 | 2 | 1 | 400 kNm | $M_0$ - $\omega$ |
| C4 | Dickin and Laman (2003) | $d/l = 0.33$ | Rough steel rectangular pier | 6 | 3 | 1 | | $M_0$ - $\omega$ |
| C5 | | $d/l = 0.6$ | | 6 | 3 | 1.8 | | |
| C6 | | $d/l = 1$ | | 6 | 3 | 3 | | |
| C7 | | $d/l = 1.33$ | | 6 | 3 | 4 | | |
| C8 | | $d/l = 2$ | | 6 | 3 | 6 | | |
| C9 | | $d/l = 0.33$ | | 6 | 3 | 1 | | |
| C10 | | $d/l = 1$ | | 6 | 3 | 3 | | |

Table 2 Continued

| Test No. | Reference | Pile No. in reference | Pile type | $e$ (m) | $l$ (m) | $d$ (m) | Measured $M_u$ or $T_u$ | Measured curves |
|---|---|---|---|---|---|---|---|---|
| C11 | Dickin and Laman (2003) | $d/l$ = 1.33 | Rough steel rectangular pier | 6 | 3 | 4 | | $M_0$ - $\omega$ |
| C12 | | $d/l2$ | | 6 | 3 | 6 | | |
| **Model tests** | | | | | | | | |
| M1 | Petrasovits and Awad (1972) | $l/d$ = 14.3 | Smooth pile | 0.14 | 0.5 | 0.035 | 553.7N | $T$ - $u_t$ |
| M2 | | $l/d$ = 25.0 | | 0.14 | 0.5 | 0.020 | 301.4 N | |
| M3 | | $l/d$ = 38.5 | | 0.14 | 0.5 | 0.013 | 245 N | |
| M4 | Adams and Radhakrishna (1973) | $d$ = 101.6 mm | Steel pipe pile | 0.3175 | 0.4445 | 0.1016 | | $T$ - $u_0$ |
| M5 | | $d$ = 101.6 mm | | 0.3175 | 0.4445 | 0.1016 | | |
| M6 | | $d$ = 76.2 mm | Steel pipe pile filled with cement grout | 0.3175 | 0.4445 | 0.0762 | | |
| M7 | | $d$ = 50.8 mm | | 0.3175 | 0.4445 | 0.0508 | | |
| M8 | Meyerhof *et al*. (1981) | Loose sand | Rough steel pile | 0 | 0.2 | 0.0125 | 11N | $T$ - $u_0$ |
| M9 | | Dense sand | | 0 | 0.2 | 0.0125 | 40N | |
| M10 | Chari and Meyerhof (1983) | | Smooth steel pipe pile | 0.075 | 0.991 | 0.075 | 2050N | $T$ - $u_t$ |
| M11 | Swane (1983) | DSSU1 | Aluminum circular pile | 0.05 | 0.4 | 0.024 | | $T$ - $u_0$ |
| M12 | | DSSU2 | | 0.05 | 0.4 | 0.024 | | |
| M13 | | LSSU1 | | 0.05 | 0.4 | 0.024 | | |
| M14 | Prasad and Chari (1996) | 1 | Smooth steel pipe pile | 24 | 0.612 | 0.102 | 425 Nm | $M_0$ - $\omega$ |
| M15 | | 2 | | 24 | 0.612 | 0.102 | 1200 Nm | |
| M16 | | 5 | | 24 | 0.51 | 0.102 | 325 Nm | |
| M17 | | 6 | | 24 | 0.51 | 0.102 | 800 Nm | |
| M18 | Prasad and Chari (1999 ) | $D_r$ = 25% | Smooth steel pipe pile | 0.15 | 0.612 | 0.102 | 620N | $T$ - $u_t$ |
| M19 | | $D_r$ = 50% | | 0.15 | 0.612 | 0.102 | 1040N | |
| M20 | | $D_r$ = 75% | | 0.15 | 0.612 | 0.102 | 1790N | |
| M21 | Qin and Guo (2007) | TS1 | Aluminum pipe pile | 0.115 | 0.5 | 0.032 | 740N | $T$ - $u_{0,}$ $M(z)$, $u(z)$ |
| M22 | | TC1 | | 0.115 | 0.5 | 0.032 | 810 N | |
| M23 | | TC2 | | 0.115 | 0.5 | 0.032 | 820 N | |

Table 3 Soil properties and deduced parameters

| Test No. | Soil type | $D_r$ (%) | $\phi'_s$ (°) | $\gamma'_s$ (kN/m$^3$) | $A_r$ (kN/m$^3$) | $N_g$ | $k_0$ (MN/m$^4$) | $k$ (MN/m$^3$) |
|---|---|---|---|---|---|---|---|---|
| | | | **Full-scale field tests** | | | | | |
| F1 | Loose sand | 45 | 37.1 | 17.2 | 400 | 1.43 | 26.1 | 41.0 |
| F2 | Very loose sand | 22 | 32.6 | 16.4 | 150 | 0.82 | 3.0 | 4.5 |
| F3 | Loose sand | 31 | 34.4 | 16.7 | 278 | 1.29 | 5.1 | 9.3 |
| F4 | Medium dense sand | 56 | 39.2 | 17.6 | 512 | 1.48 | 31.1 | 49.5 |
| F5 | Loose sand | 43 | 36.7 | 17.1 | 575 | 2.13 | 31.1 | 49.0 |
| F6 | Dense crushed stone | 86 | 49.8 | 19.2 | 600 | 0.56 | 20.1 | 30.5 |
| F7 | Dense gravelly sand | 85 | 42.7 | 19.7 | 560 | 1.05 | 31.1 | 49.0 |
| F8 | Silt sand (0~0.9m) and silty sand gravely layers (0.9~5.5m) | 77 (0~0.9 m) | 40† | 16.5 | 480 | 1.38 | 26.5 | 94.0 |
| F9 | | 88 (0.9~5.5 m) | 40† | 16.5 | 350 | 1.00 | 25.0 | 94.0 |
| F10 | Silt sand (0~1.8 m) and silty sand with gravely layers (1.8~5.5m) | 38 (0~1.8 m) | 38† | 16.5 | 360 | 1.23 | 25.0 | 99.0 |
| F11 | | 92 (1.8~5.5 m) | 38† | 16.5 | 360 | 1.23 | 50.0 | 129.0 |
| F12 | Fine to medium sand with silt | | 34 | 11.0 | 140 | 1.00 | 7.5 | 26.0 |
| F13 | Silty sand | | 30 | 8.2 | 222.5 | 3.00 | 38.0 | 34.0 |
| F14 | Clayey sand | 30~35 | 35.4 | 14.5 | 950.0 | 4.65 | 220.0 | 184.0 |
| F15 | | | 35.4 | 14.5 | 365 | 1.80 | 200.0 | 234.0 |
| F16 | | | 35.4 | 14.5 | 800 | 3.90 | 200.0 | 304.0 |
| | | | **Centrifuge tests** | | | | | |
| C1 | Uniform fine grained dry medium dense to dense sand | 60 | 36 | 16.3 | 340 | 1.41 | 3.0 | 10.0 |
| C2 | | 60 | 36 | 16.3 | 280 | 1.16 | 3.0 | 10.0 |
| C3 | Dry dense sand | | 46.1 | 16.4 | 621.7 | 1.00 | 25.0 | 34.4 |
| C4 | Fine clean dry dense sand | 85 | 49 | 16.4 | 532 | 0.63 | 45.0 | 55.5 |
| C5 | | 85 | 49 | 16.4 | 490 | 0.58 | 45.0 | 85.5 |
| C6 | | 85 | 49 | 16.4 | 385 | 0.46 | 35.0 | 50.5 |
| C7 | | 85 | 49 | 16.4 | 375 | 0.45 | 35.0 | 48.5 |
| C8 | | 85 | 49 | 16.4 | 365 | 0.44 | 35.0 | 48.5 |
| C9 | Fine clean dry loose sand | 37 | 39 | 14.6 | 180 | 0.64 | 6.0 | 10.85 |
| C10 | | 37 | 39 | 14.6 | 145 | 0.51 | 6.0 | 12.5 |
| C11 | | 37 | 39 | 14.6 | 125 | 0.44 | 6.0 | 12.5 |
| C12 | | 37 | 39 | 14.6 | 120 | 0.43 | 6.0 | 9.4 |

Table 3 Continued

| Test No. | Soil type | $D_r$ (%) | $\phi'_s$ (°) | $\gamma'_s$ (kN/m$^3$) | $A_r$ (kN/m$^3$) | $N_g$ | $k_0$ (MN/m$^4$) | $k$ (MN/m$^3$) |
|---|---|---|---|---|---|---|---|---|
| | | | **Model tests** | | | | | |
| M1 | Cohesionless soil | 84 | 37.2 | 17.6 | 820.5 | 2.83 | 90.0 | 34.0 |
| M2 | | 84 | 37.2 | 17.6 | 850 | 2.93 | 95.0 | 30.0 |
| M3 | | 84 | 37.2 | 17.6 | 1050 | 3.62 | 97.0 | 33.0 |
| M4 | Uniformly graded silica sand | 89 | 31 | 15.7 | 112.5 | 0.73 | 100.0 | 30.0 |
| M5 | | 100 | 45 | 17.6 | 416 | 0.70 | 450.0 | 140.0 |
| M6 | | 100 | 45 | 17.6 | 450 | 0.75 | 500.0 | 160.0 |
| M7 | | 100 | 45 | 17.6 | 610 | 1.02 | 800.0 | 240.0 |
| M8 | Well graded medium to coarse angular sand | 35 | 35 | 14‡ | 250 | 1.31 | 51.2 | 4.8 |
| M9 | | 70 | 50 | 15.2‡ | 950 | 1.09 | 231.2 | 28.0 |
| M10 | Coarse uniform angular dry sand | 82 | 46 | 15 | 410 | 0.73 | 20.0 | 10.0 |
| M11 | Dry medium grained quartz sand | 88 | 38 | 16.12 | 1210 | 4.25 | 107 | 33 |
| M12 | | 88 | 38 | 16.12 | 1360 | 4.77 | 107 | 33 |
| M13 | | 44 | 33.5 | 15.12 | 380 | 2.09 | 87 | 23 |
| M14 | Well graded angular medium dry sand | 45 | 36 | 17 | 420 | 1.66 | 32.1 | 12.0 |
| M15 | | 80 | 44.5 | 18.6 | 630 | 1.25 | 32.1 | 15.0 |
| M16 | | 45 | 36 | 17 | 630 | 2.50 | 40.0 | 15.0 |
| M17 | Crushed stone | 80 | 49 | 18.5 | 755 | 0.80 | 65.0 | 28.0 |
| M18 | Well graded angular dry sand | 25 | 35 | 16.5 | 306 | 1.36 | 9.24 | 3.88 |
| M19 | | 50 | 41 | 17.3 | 340 | 0.85 | 48.2 | 12.05 |
| M20 | | 75 | 45.5 | 18.3 | 890 | 1.36 | 47.5 | 16.96 |
| M21 | Dry medium grained quartz sand | 89 | 38 | 16.27 | 1050 | 3.65 | 91.0 | 30.0 |
| M22 | | 89 | 38 | 16.27 | 1200 | 4.17 | 91.0 | 36.5 |
| M23 | | 89 | 38 | 16.27 | 1225 | 4.26 | 91.0 | 36.5 |

†Average values of the two layers; ‡ Reported by Prasad and Chari (1999)

mission pole foundations. Each pole consisted of top and bottom sections with diameters of 0.779 m and 0.740 m (an average diameter $d$ of 0.76 m). The two parts were joined together by bolted connections. The typical cross section of the pole was a 12-sided polygon. The embedded length $l$ of the pole varied from 2.36 m to 3.2 m. The lateral loads were applied at an eccentricity $e$ of approximately 23.0 m to investigate the responses of pole foundations under a large moment. Each pole was instrumented to measure the applied load at the top of pole and deflections near the ground line. The rotation of the pole was determined from the deflection of the pole at two different distances. Ten strain gauges were installed at different sections of the pole to measure distribution of the bending moment at selected depths. Lateral load was applied in an incremental manner until it reached the safe structural capacity of the pole or it induced a large deflection at ground line.

The poles were tested in four different types of backfills, namely, sand, in-situ gravelly sand, crushed stone and flowable material, respectively. The loose to medium dense sand backfill (F1-F5) had a relative density $D_r$ of 22%-56%, an effective unit weight $\gamma'_s$ of 16.4-17.6 kN/m$^3$and an effective internal frictional angle $\phi'_s$ of 32.6°-39.2°, respectively. The dense crushed stone (F6) and in-situ gravelly sand (F7) have a relative density of 85% with larger effective internal frictional angles of 49.8° and 42.7°.

The pole test F1 (with $d$ = 0.7545 m, $l$ = 3.2 m, and $e$ = 22.25 m) was tested in loose sand backfill. The measured $M_0 - \omega$ curve is plotted in Fig. 2(a). The measured bending moment distribution with depth and pole displacement at a groundline moment $M_0$ of 245 kNm, 365 kNm, 485 kNm, and 685 kNm are plotted in Figs. 2(b)-(c). The measured soil pressure on the pole using pressure cells at $M_0$ = 685 kNm is plotted in Fig. 2(d).

The back-calculated pole curves are also plotted in Figs. 2(a)-(d), which are based on $A_r$ = 400 kN/m$^3$, $k_0$ = 26.1 MN/m$^4$, and $k$ = 41.0 MN/m$^3$. The following features are observed.

(1) Taking the same value of $A_r$, back calculation using the solutions with a constant $k$ gives a better match with the measured $M_0 - \omega$ relationships (see Fig. 2(a)).

(2) Pile deflections are well predicted (see Fig. 2(a), (c)), while the bending moment distributions are slightly overestimated (see Fig. 2(b)) especially at high-load levels using either $k$.

(3) The calculated $M_0$ = 682.4 kNm (Gibson $k$) is close to the measured value of 685 kNm at ground line, and the calculated $M_0$ is 751.65 kNm (constant $k$) at the tip-yield state. The measured soil pressure profile and the on-pile force profiles for both $k$ at tip-yield state are plotted in Fig. 2(d). The soil pressure distribution proposed by Prasad and Chari (1999) was included for comparison as well. The measured data fall within the zones enclosed by the individual soil pressure profile, further confirming that the pole was at pre-tip yield or close to tip-yield state.

(4) The ultimate ground line moment of the pole was calculated as 875.7 kNm, which is 2.4% greater than the reported ultimate moment of 855 kNm at 5° rotation of the pole.

## 4. Discussions

### *4.1 Reliability of the back calculation*

The 51 pile tests are divided into three groups based on the number of measured pile response curves: (1) eight tests (F1, F12-13, C1-2 and M21-23) with two or more curves; (2) thirteen tests

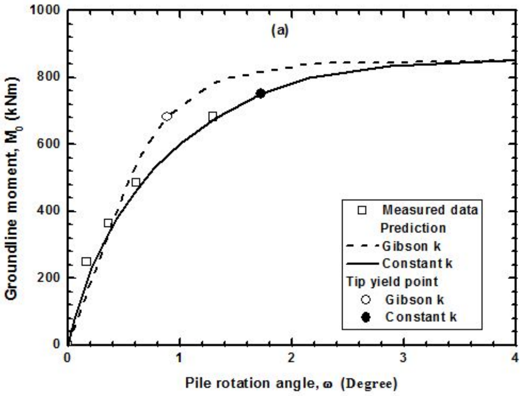


(a)

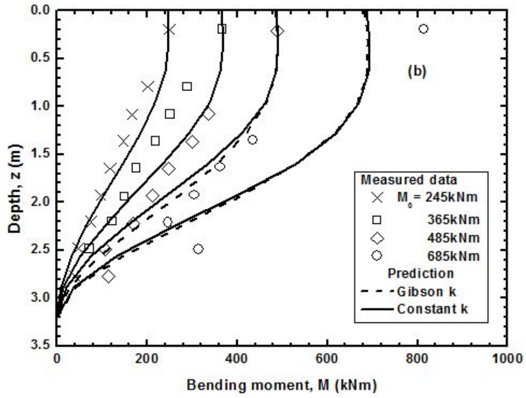


(b)

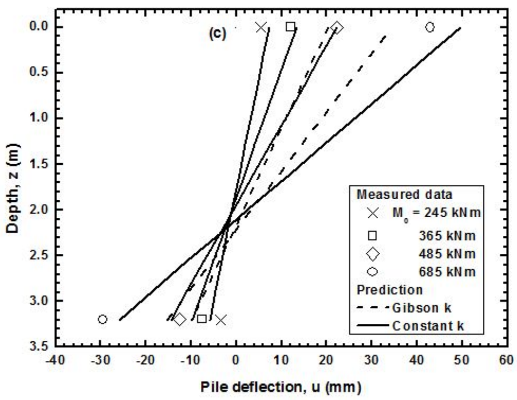


(c)

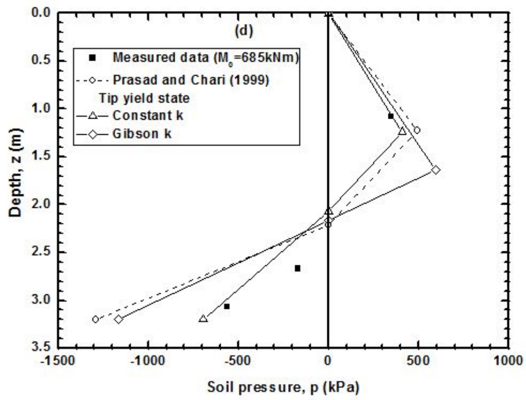


(d)

Fig. 2 Predicted and measured (Haldar *et al*. 2000) response of pile F1

(F14-16 and C3-12) with the $T_t - u_0(u_t)$ or $M_0 - \omega$ curve ranging from elastic to a clear ultimate state; and (3) the remaining thirty tests having only $T_t - u_0(u_t)$ or $M_0 - \omega$ curve, but without clear indication of ultimate state. In order to investigate the effect of $e/l$ on the pile responses, the measured $T_t - u_0(u_t)$ and $M_0 - \omega$ data for each test were normalised by $A_r dl^2$, $A_r l/k$, $A_r dl^3$ and $A_r/k$, respectively, using the deduced $A_r$ and constant $k$ in Table 3. The normalised lateral load versus groundline displacement or pile-head displacement data are plotted in Fig. 10(a) and normalised moment versus groundline rotation data in Fig. 10(b).The deduced $A_r$, $k$ and $k_0$ for the 21 tests in the first and second groups are warranted and reliable because of the good agreement between the back-calculated curves with the measured ones shown in Figs. 2-9. The back-calculated results in the third group may vary if additional measured responses are available.

The back calculation shows that the solution with constant $k$ generally offers a better match against the measured responses of the piles than that based on Gibson $k$, in light of the linear limiting force profile with the same gradient $A_r$. However, tests M3, M8, M10 and M18 were not well predicted, owing to stress hardening characteristics (Guo 2008). The following discussions are limited to back calculation using the solution with constant $k$.

### 4.2 Effect of e/l on nonlinear pile response, pile capacity $T_0$ and $M_0$

The non-dimensional $T_t/(A_r d l^2)$ – $u_0 k/(A_r l)$ and $M_0(A_r d l^3)$ – $(-\omega k/A_r)$ curves at the $e/l$ ratios calculated from Table 2 were obtained from the solution with constant $k$ and are plotted as solid lines in Figs. 10(a)-(b). It can be seen that at a specific $e/l$, the normalised measured $T_t - u_0(u_t)$ or $M_0 - \omega$ curves merge or fall within a very narrow band around the solid lines, regardless of soil properties. The ratio $e/l$ has a significant impact on the normalised load $T_t/(A_r d l^2)$, which reduces with the increase of $e/l$. For instance, at $u_0 k/(A_r l) = 2$, the $T_t/(A_r d l^2)$ reduces about 40% from 0.09 to 0.053 as $e/l$ increases from 0 to 0.8. On the other hand, the normalised moment $M_0(A_r d l^3)$ increases with the increasing $e/l$. At $-\omega k/A_r = 2$, $M_0(A_r d l^3)$ increases by 35% from 0.052 to 0.07 with $e/l$ increasing from 2 to 47.

The measured ultimate lateral capacities of 29 tests were reported in terms of either lateral load $T_u$ or groundline moment $M_u$ and are presented in Table 2. These ultimate capacities were determined as: (1) the load at which the lateral load - pile head displacement curve becomes linear or substantially linear (Meyerhof *et al*. 1981, Chari and Meyerhof 1983, Prasad and Chari 1996,

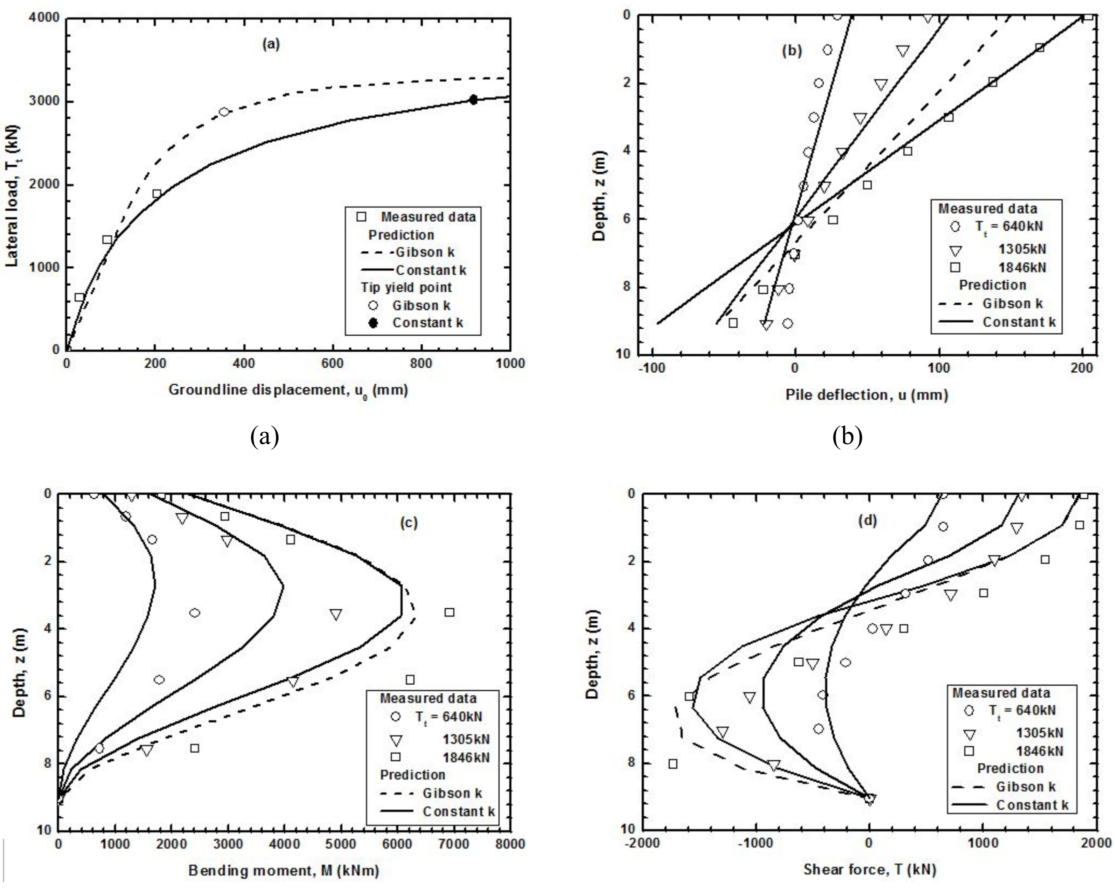


(a) (b)

(c) (d)

Fig. 3 Predicted and measured (Georgiadis *et al*. 1992) response of pile C1

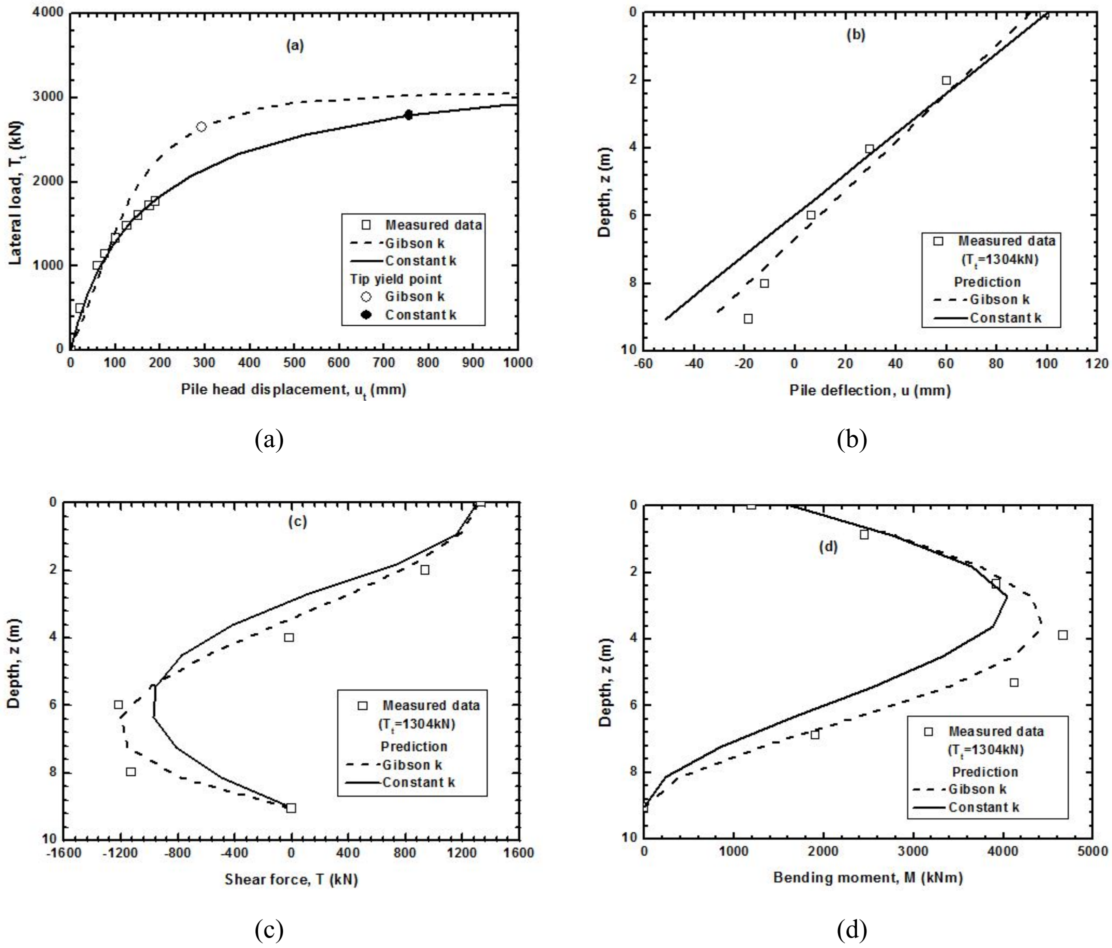


Fig. 4 Predicted and measured (Georgiadis *et al*. 1992) response of pile C2

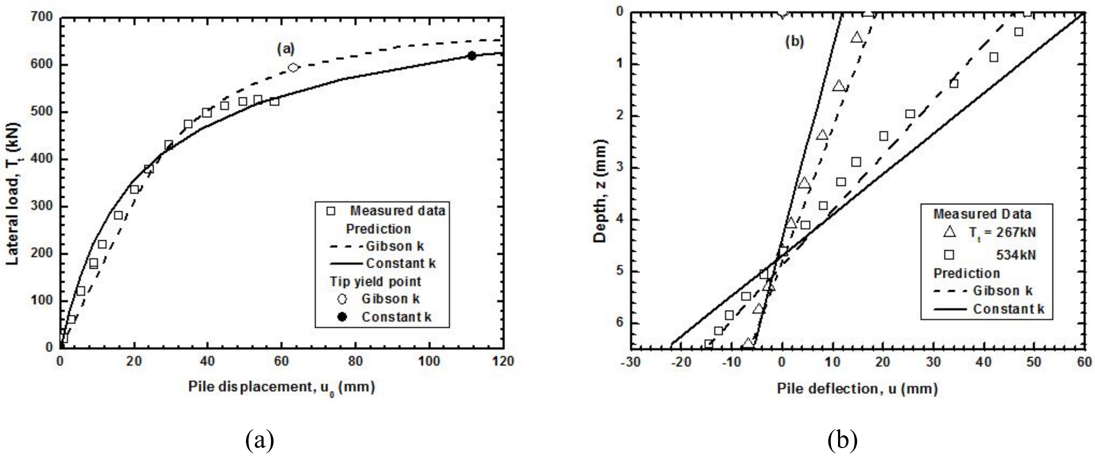


Fig. 5 Predicted and measured (Ismael and Klym1981) response of pile F12

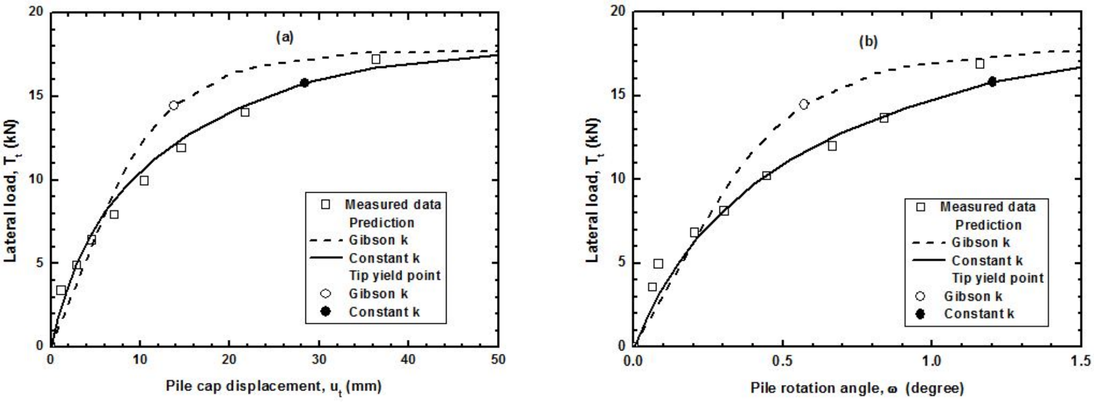


(a) (b)

Fig. 6 Predicted and measured (Pender and Matuschka 1988) response of pile F13

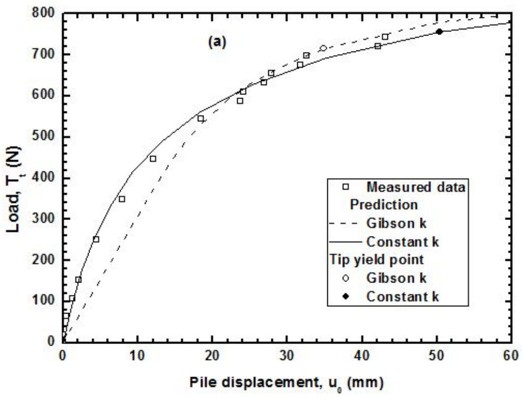


(a)

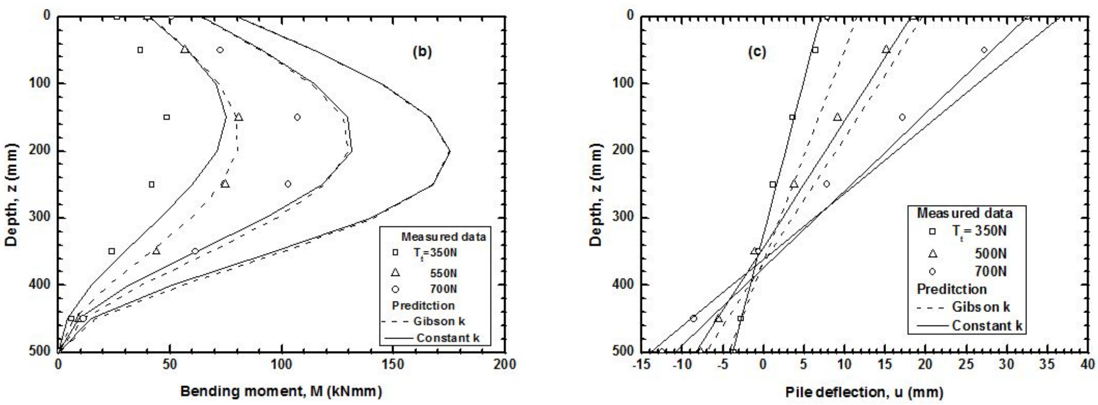


(b) (c)

Fig. 7 Predicted and measured (Qin and Guo 2007) response of pile M21

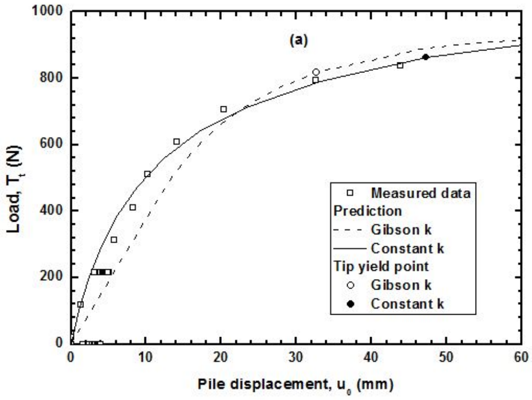


(a)

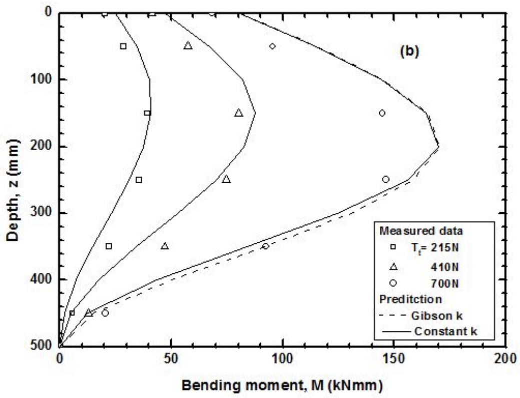


(b)

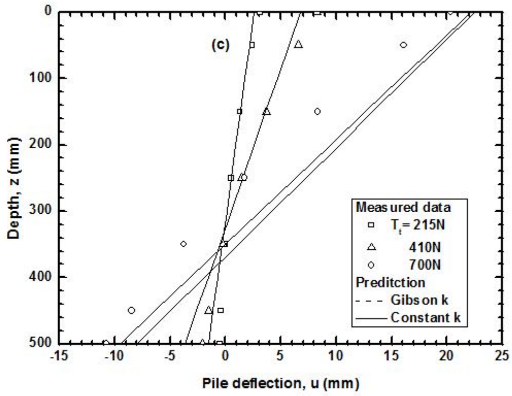


(c)

Fig. 8 Predicted and measured (Qin and Guo 2007) response of pile M22

1999, Lee *et al*. 2010); or (2) the lateral load/moment at a rotation angle of 3.5°-5.5° (Laman *et al*. 1999, Dickin and Laman 2003) or 5° (Haldar *et al*. 2000). Figs. 11(a)-(b) show the normalised measured pile capacity $T_0(A_r dl^2)$ and moment $M_0(A_r dl^3)$ against normalised eccentricity $e/l$, respectively, in which the theoretical curves by Guo (2008) at tip-yield and yield at rotation point (YRP) are also plotted. Fig. 11(a) shows that the measured ultimate lateral load $T_u$ is generally less than the calculated capacity at tip-yield state. By contrast, Fig. 11(b) shows that the measured ultimate ground line moment $M_u$ falls in the range of the capacity between tip-yield state and yield at rotation point, except tests M14 and M16. As reported the measured values of $M_u$ for the two tests were obtained at a much lower pile rotation angle $\omega$ of around 1.5°. Overall the pile capacity at the yield at rotation point provides a good upper bound.

### *4.3 Estimation of average shear modulus $\bar{G}_s$*

The modulus of subgrade reaction $kd$ is related to the average shear modulus $\overline{G_s}$ of the sand over the embedded length of the pile via Eq. (2). Conversely, the shear modulus of the sands can be deduced from the back-calculated modulus of subgrade reaction. On the other hand, the small strain shear modulus $G_{\max}$ (for which many empirical equations are available) may be used as a universal reference or benchmark value of stiffness when applied to foundation systems (Poulos *et al.* 2001). For instance, Seed and Idriss (1970) and Seed *et al*. (1986) proposed the following

$$G_{\max} = 218.8 K_{2,\max} (\sigma'_m)^{0.5} \tag{5}$$

where $G_{\max}$ is in kPa, $\sigma'_m$ is the effective mean stress in kPa, which is related to the vertical effective stress $\sigma'_v$ by $\sigma'_m = [(1 + 2K_0 / 3]\ \sigma'_v$, and to the coefficient of earth pressure at rest $K_0 = 1 - \sin \varphi'_s$ (Jaky 1944). In this study, the $\sigma'_v$ is taken as the average vertical effective stress along the embedded length of the pile. $K_{2,\max}$ is a dimensionless modulus coefficient that depends on the relative density $D_r$in percent (Seed and Idriss 1970, Yan and Byrne 1992)

$$K_{2,\max} = 3.5 (D_r)^{2/3} \tag{6}$$

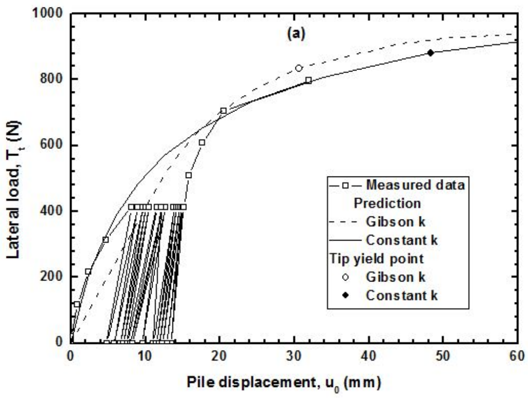


(a)

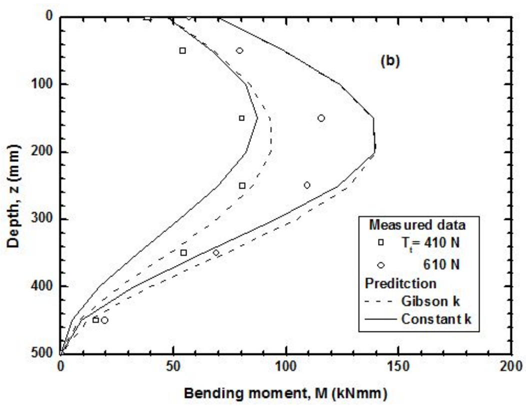


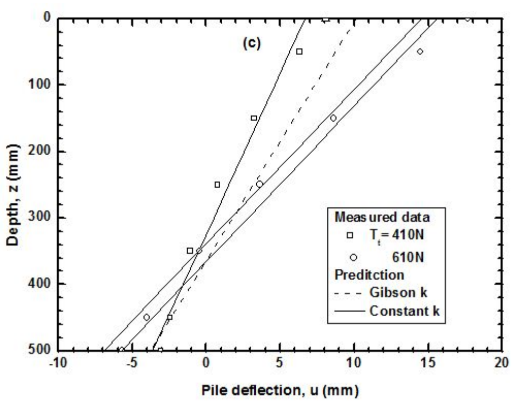


(b) (c)

Fig. 9 Predicted and measured (Qin and Guo 2007) response of pile M23

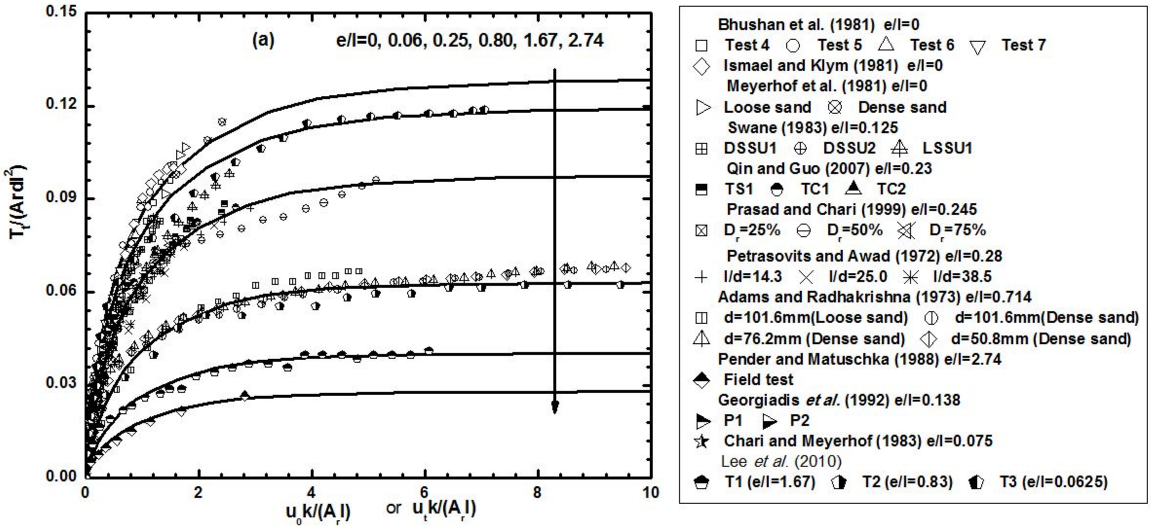


(a) Normalised load and displacement relationship

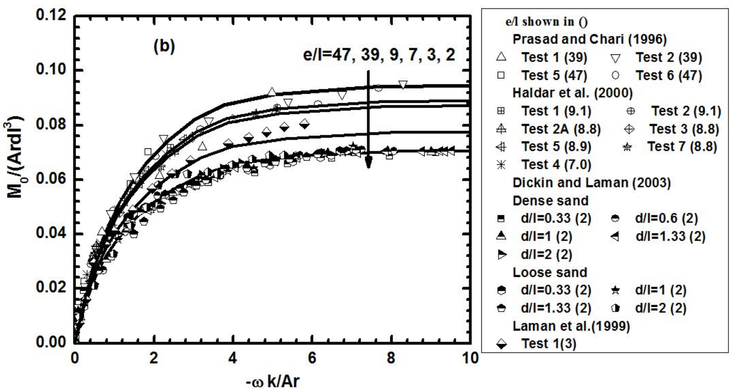


(b) Normalised moment and rotation relationship

Fig. 10 Normalised load, displacement and rotation: measured versus predicted

Seed *et al*. (1986) stated that the values of range from about 30 for loose sands to about 75 for dense sands and they are 1.35 - 2.5 times greater for gravels than for sands. Therefore, the values of $K_{2,\max}$ calculated from Eq. (6) for tests F6-F11 (piles tested in dense crushed stone, gravelly sand and gravelly silty sand) are doubled (the approximate average value of 1.35 - 2.5).

The ratio $kd/\overline{G}_s$ was calculated from Eq. (2), which depends only on the loading characteristics, loading eccentricity, pile diameter and embedded length. The average shear modulus $\overline{G}_s$ was subsequently obtained from the back-calculated $k$ for each pile. Likewise, the $G_{\max}$ was calculated from Eqs. (5) and (6). The second (MTD2) and fourth methods (MTD4) presented by Wichtmann and Triantafyllidis (2009) (see footnote of Table 4) were also used to calculate the $G_{\max}$ and to provide an order-of-magnitude check of the deduced $G_{\max}$ from Eqs. (5) and (6). These results are presented in Table 4 and summarised as follows.

Table 4 Average shear modulus $\overline{G}_s$ and $G_{max}$

| Test No. | $\gamma$ | $K_1(\gamma)$ | $K_0(\gamma)$ | $kd/\overline{G}_s$ | $K_0$ | $\sigma'_m$ (kPa) | MTD2[*] | MTD4[‡] | | Eqs. (5) and (6) | | $\overline{G}_s$ (MPa) | $\overline{G}_s/G_{max}$ [†] |
|---|---|---|---|---|---|---|---|---|---|---|---|---|---|
| | | | | | | | $G_{max}$ (MPa) | $K_{2,max}$ | $G_{max}$ (MPa) | $K_{2,max}$ | $G_{max}$ (MPa) | | |
| **Full-scale field tests and centrifuge tests** | | | | | | | | | | | | | |
| F1 | 0.440 | 1.946 | 1.033 | 5.49 | 0.397 | 16.453 | 38.014 | 40.850 | 36.254 | 44.280 | 39.299 | 5.639 | 0.143 |
| F2 | 0.565 | 1.412 | 0.825 | 6.21 | 0.461 | 13.242 | 28.047 | 33.382 | 26.578 | 27.480 | 21.880 | 0.551 | 0.025 |
| F3 | 0.565 | 1.412 | 0.825 | 6.21 | 0.435 | 13.117 | 30.298 | 36.254 | 28.729 | 34.539 | 27.370 | 1.138 | 0.042 |
| F4 | 0.550 | 1.462 | 0.846 | 6.13 | 0.368 | 13.189 | 37.263 | 44.573 | 35.417 | 51.230 | 40.707 | 6.147 | 0.151 |
| F5 | 0.549 | 1.468 | 0.848 | 6.12 | 0.402 | 13.322 | 33.796 | 40.183 | 32.090 | 42.958 | 34.306 | 6.077 | 0.177 |
| F6 | 0.553 | 1.452 | 0.842 | 6.14 | 0.236 | 12.109 | 88.431 | 55.258 | 84.144 | 68.192 | 103.840 | 3.767 | 0.036 |
| F7 | 0.549 | 1.468 | 0.848 | 6.12 | 0.322 | 13.978 | 94.113 | 54.888 | 89.800 | 67.662 | 110.698 | 6.077 | 0.055 |
| F8 | 0.119 | 8.263 | 2.259 | 3.27 | 0.357 | 25.931 | 127.451 | 55.258 | 123.134 | 68.192 | 151.956 | 17.536 | 0.115 |
| F9 | 0.178 | 5.408 | 1.864 | 3.76 | 0.357 | 25.931 | 127.451 | 55.258 | 123.134 | 68.192 | 151.956 | 22.878 | 0.151 |
| F10 | 0.178 | 5.408 | 1.864 | 3.76 | 0.384 | 26.751 | 149.408 | 50.996 | 144.276 | 61.858 | 175.006 | 24.095 | 0.138 |
| F11 | 0.237 | 3.967 | 1.590 | 4.19 | 0.384 | 26.751 | 149.408 | 50.996 | 144.276 | 61.858 | 175.006 | 37.528 | 0.214 |
| F12 | 0.153 | 6.350 | 2.012 | 3.56 | 0.441 | 22.078 | | | | | | | |
| F13 | 0.690 | 1.072 | 0.671 | 6.91 | 0.500 | 5.385 | | | | | | | |
| F14 | 0.588 | 1.338 | 0.793 | 6.34 | 0.421 | 5.340 | 19.943 | 36.739 | 18.576 | 35.644 | 18.023 | 11.605 | 0.644 |
| F15 | 0.278 | 3.336 | 1.444 | 4.47 | 0.421 | 10.680 | 27.816 | 36.739 | 26.270 | 35.644 | 25.488 | 20.946 | 0.822 |
| F16 | 0.200 | 4.769 | 1.751 | 3.93 | 0.421 | 10.680 | 27.816 | 36.739 | 26.270 | 35.644 | 25.488 | 30.964 | 1.215 |
| C1 | 0.159 | 6.111 | 1.976 | 3.61 | 0.412 | 44.855 | 69.108 | 45.952 | 67.338 | 53.642 | 78.606 | 3.028 | 0.039 |
| C2 | 0.178 | 5.417 | 1.866 | 3.76 | 0.412 | 44.855 | 69.108 | 45.952 | 67.338 | 53.642 | 78.606 | 3.258 | 0.041 |
| C3 | 0.910 | 0.704 | 0.480 | 8.08 | 0.279 | 8.522 | | | | | | | |
| C4 | 0.595 | 1.318 | 0.784 | 6.38 | 0.245 | 12.223 | 44.122 | 54.888 | 41.987 | 67.662 | 51.758 | 8.700 | 0.168 |
| C5 | 1.071 | 0.535 | 0.381 | 8.92 | 0.245 | 12.223 | 44.122 | 54.888 | 41.987 | 67.662 | 51.758 | 17.253 | 0.333 |
| C6 | 1.784 | 0.187 | 0.149 | 12.51 | 0.245 | 12.223 | 44.122 | 54.888 | 41.987 | 67.662 | 51.758 | 12.111 | 0.234 |
| C7 | 2.379 | 0.086 | 0.072 | 15.42 | 0.245 | 12.223 | 44.122 | 54.888 | 41.987 | 67.662 | 51.758 | 12.580 | 0.243 |

Table 4 Continued

| Test No. | $\gamma$ | $K_1(\gamma)$ | $K_0(\gamma)$ | $kd / \overline{G}_s$ | $K_0$ | $\sigma'_m$ (kPa) | MTD2* | MTD4‡ | | Eqs. (5) and (6) | | $\overline{G}_s$ (MPa) | $\overline{G}_s / G_{max}$ † |
|---|---|---|---|---|---|---|---|---|---|---|---|---|---|
| | | | | | | | $G_{max}$ (MPa) | $K_{2,max}$ | $G_{max}$ (MPa) | $K_{2,max}$ | $G_{max}$ (MPa) | | |
| C8 | 3.569 | 0.021 | 0.018 | 21.16 | 0.245 | 12.223 | 44.122 | 54.888 | 41.987 | 67.662 | 51.758 | 13.754 | 0.266 |
| C9 | 0.595 | 1.318 | 0.784 | 6.38 | 0.371 | 12.712 | 31.434 | 38.204 | 29.803 | 38.863 | 30.317 | 1.701 | 0.056 |
| C10 | 1.784 | 0.187 | 0.149 | 12.51 | 0.371 | 12.712 | 31.434 | 38.204 | 29.803 | 38.863 | 30.317 | 2.998 | 0.099 |
| C11 | 2.379 | 0.086 | 0.072 | 15.42 | 0.371 | 12.712 | 31.434 | 38.204 | 29.803 | 38.863 | 30.317 | 3.242 | 0.107 |
| C12 | 3.569 | 0.021 | 0.018 | 21.16 | 0.371 | 12.712 | 31.434 | 38.204 | 29.803 | 38.863 | 30.317 | 2.666 | 0.088 |
| | | | | | | | **Model tests** | | | | | | |
| M1 | 0.102 | 9.702 | 2.412 | 3.11 | 0.395 | 2.627 | 20.952 | 54.520 | 19.333 | 67.131 | 23.804 | 0.382 | 0.016 |
| M2 | 0.058 | 17.136 | 2.966 | 2.65 | 0.395 | 2.627 | 20.952 | 54.520 | 19.333 | 67.131 | 23.804 | 0.227 | 0.010 |
| M3 | 0.038 | 26.444 | 3.395 | 2.37 | 0.395 | 2.627 | 20.952 | 54.520 | 19.333 | 67.131 | 23.804 | 0.181 | 0.008 |
| M4 | 0.374 | 2.364 | 1.173 | 5.09 | 0.485 | 2.291 | 20.279 | 56.371 | 18.670 | 69.769 | 23.107 | 0.599 | 0.026 |
| M5 | 0.374 | 2.364 | 1.173 | 5.09 | 0.293 | 2.068 | 20.704 | 60.524 | 19.042 | 75.405 | 23.724 | 2.795 | 0.118 |
| M6 | 0.281 | 3.292 | 1.433 | 4.49 | 0.293 | 2.068 | 20.704 | 60.524 | 19.042 | 75.405 | 23.724 | 2.715 | 0.114 |
| M7 | 0.187 | 5.126 | 1.816 | 3.83 | 0.293 | 2.068 | 20.704 | 60.524 | 19.042 | 75.405 | 23.724 | 3.184 | 0.134 |
| M8 | 0.067 | 14.842 | 2.825 | 2.75 | 0.426 | 0.865 | 8.505 | 37.551 | 7.640 | 37.450 | 7.619 | 0.022 | 0.003 |
| M9 | 0.067 | 14.842 | 2.825 | 2.75 | 0.234 | 0.744 | 10.387 | 49.460 | 9.333 | 59.447 | 11.217 | 0.127 | 0.011 |
| M10 | 0.093 | 10.655 | 2.502 | 3.02 | 0.281 | 3.868 | 24.896 | 53.787 | 23.146 | 66.061 | 28.428 | 0.248 | 0.009 |
| M11 | 0.078 | 12.724 | 2.675 | 2.87 | 0.384 | 1.901 | 18.419 | 55.999 | 16.892 | 69.245 | 20.888 | 0.276 | 0.013 |
| M12 | 0.078 | 12.724 | 2.675 | 2.87 | 0.384 | 1.901 | 18.419 | 55.999 | 16.892 | 69.245 | 20.888 | 0.276 | 0.013 |
| M13 | 0.078 | 12.724 | 2.675 | 2.87 | 0.448 | 1.911 | 13.417 | 40.516 | 12.256 | 43.622 | 13.195 | 0.192 | 0.015 |
| M14 | 0.316 | 2.880 | 1.325 | 4.72 | 0.412 | 3.164 | 17.228 | 40.850 | 15.897 | 44.280 | 17.232 | 0.259 | 0.015 |
| M15 | 0.316 | 2.880 | 1.325 | 4.72 | 0.299 | 3.032 | 21.853 | 53.057 | 20.214 | 64.982 | 24.758 | 0.324 | 0.013 |
| M16 | 0.379 | 2.326 | 1.161 | 5.12 | 0.412 | 2.636 | 15.784 | 40.850 | 14.512 | 44.280 | 15.731 | 0.299 | 0.019 |
| M17 | 0.379 | 2.326 | 1.161 | 5.12 | 0.245 | 2.344 | 19.313 | 53.057 | 17.773 | 64.982 | 21.768 | 0.558 | 0.026 |
| M18 | 0.237 | 3.970 | 1.591 | 4.19 | 0.426 | 3.118 | 14.405 | 34.332 | 13.265 | 29.925 | 11.562 | 0.094 | 0.008 |

Table 4 Continued

| Test No. | $\gamma$ | $K_1(\gamma)$ | $K_0(\gamma)$ | $kd/\overline{G}_s$ | $K_0$ | $\sigma'_m$ (kPa) | MTD2[*] | MTD4[‡] | | Eqs. (5) and (6) | | $\overline{G}_s$ (MPa) | $\overline{G}_s/G_{max}$ [†] |
|---|---|---|---|---|---|---|---|---|---|---|---|---|---|
| | | | | | | | $G_{max}$ (MPa) | $K_{2,max}$ | $G_{max}$ (MPa) | $K_{2,max}$ | $G_{max}$ (MPa) | | |
| M19 | 0.237 | 3.970 | 1.591 | 4.19 | 0.344 | 2.978 | 17.416 | 42.530 | 16.060 | 47.502 | 17.937 | 0.293 | 0.016 |
| M20 | 0.237 | 3.970 | 1.591 | 4.19 | 0.287 | 2.937 | 20.798 | 51.247 | 19.217 | 62.246 | 23.341 | 0.413 | 0.018 |
| M21 | 0.090 | 10.943 | 2.528 | 3.00 | 0.384 | 2.398 | 20.728 | 56.371 | 19.100 | 69.769 | 23.639 | 0.320 | 0.014 |
| M22 | 0.090 | 10.943 | 2.528 | 3.00 | 0.384 | 2.398 | 20.728 | 56.371 | 19.100 | 69.769 | 23.639 | 0.389 | 0.016 |
| M23 | 0.090 | 10.943 | 2.528 | 3.00 | 0.384 | 2.398 | 20.728 | 56.371 | 19.100 | 69.769 | 23.639 | 0.389 | 0.016 |

*Note: [*]MTD2: $G_{\max} = A_D \dfrac{1 + D_z/100}{(a_D - D_r/100)^2} p_{atm}^{1-n} (\sigma'_m)^n$ (MPa), $A_D = 177$, $a_D = 17.3$, $n = 0.48$, $p_{atm} = 100$ kPa, atmospheric pressure, and

[‡]MTD4: $K_{2,\max} = A_{KD} \dfrac{1 + D_r/100}{(a_{KD} - D_r/100)^2}$, $A_{KD} = 6900$, $a_{KD} = 16.1$. $G_{\max} = 218.8 K_{2,\max} (\sigma'_m)^{0.5}$, (kPa). Wichtmann and Triantafyllidis (2009)

[†]$G_{max}$ calculated from Eqs. (5) and (6).

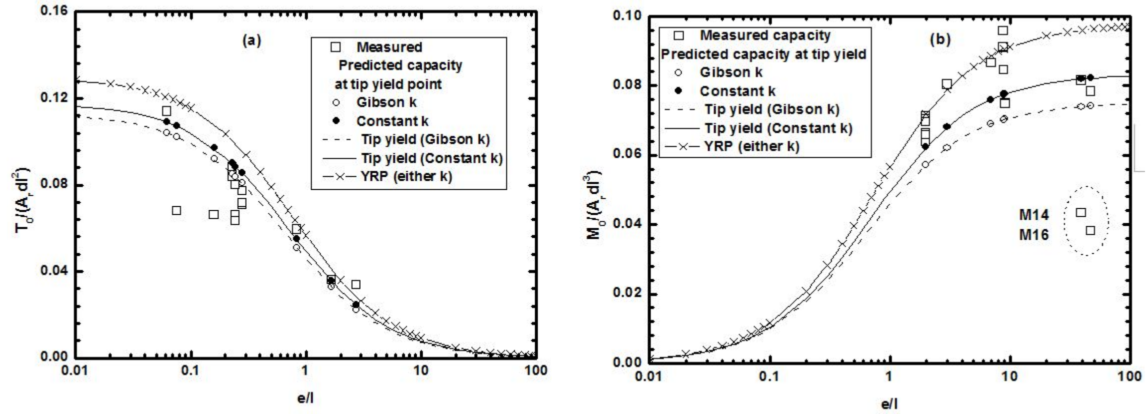


(a) (b)

Fig. 11 Normalised pile capacity at critical yield states

The full-scale field and centrifuge tests C1 and C2 have $kd/\overline{G}_s$ = 3.27 ~ 6.91, with an average of 5.0. The model tests have $kd/\overline{G}_s = 2.37-5.12$, with an average of 3.7. High values of $kd/\overline{G}_s$ (an average value of 13.32) for the centrifuge tests C4-C12 were obtained for the rectangular piers. Strictly speaking, Eq. (2) obtained from a cylindrical pile is not suitable for the rectangular pier (Basu and Salgado 2008). Therefore, the back-calculated values of the shear modulus from tests C4-C12 with a width of 1-6 m were not included in the later analysis. This may partly explain the relatively high values of $kd/\overline{G}_s$ gained from tests F1-F7 with the 12-sided polygonal pole.

With constant pile diameter and embedded length, an increasing loading eccentricity generally results in an increased ratio $kd/\overline{G}_s$. For instance, the $kd/\overline{G}_s$ increases from 3.93 to 4.47 as the eccentricity increases from 0.15 m in test F16 to 2 m in test F15. The ratio $kd/\overline{G}_s$ appears to increase with the pile diameter. For example, in the series of tests M5-M7, when the pile diameter is doubled from 0.0508 m to 0.1016 m, the $kd/\overline{G}_s$ increases by 33% from 3.83 to 5.09.

The values of $G_{\max}$ calculated using the methods proposed by Wichtmann and Triantafyllidis (2009) are within ± 25% and ± 20% of those calculated by Eqs. (5)-(6).

The ratios of $\overline{G}_s / G_{max}$ for the three tests F14-F16 (bored piles in clayey sand) are much larger than those of the other full-scale field tests. The back-calculated $\overline{G}_s$ for test F16 is even 22% higher than the calculated $G_{\max}$, owing to high plasticity (Vucetic and Dobry 1991). Thus, Eqs. (5) and (6) are not suitable for the clayey sand. The model tests M5-M7 in extremely dense sand ($D_r$ = 100%) are associated with a ratio of $\overline{G}_s / G_{\max}$ of 0.12, which is about 8.6 times the average value of 0.014 for the $\overline{G}_s / G_{\max}$ obtained from the other model tests. The $G_{\max}$ might be underestimated.

The results of the 15 tests (F14-F16, C4-C12 and M5-M7) were excluded in statistical analysis due to the reasons mentioned above, so were tests F12, F13 and C3without $D_r$ values. The deduced ratios of $\overline{G}_s / G_{\max}$ are plotted against the relative density $D_r$ for the remaining 33 tests in Fig. 12.The back-calculated $\overline{G}_s$ is approximately (3-20) % of $G_{\max}$ (with an average of 11.3%) for the 11 full-scale field tests (F1-F11) and 2 centrifuge tests (C1-C2),and (0.8-2.6) % of $G_{\max}$ (with an average of 1.4%) for the 20 model tests, indicating the impact of scale (Poulos*et al.* 2001), stress and strain level (Pestana and Salvati 2006, Guo 2012). The variation for the field tests may reflect the impact of installation for bored piles, cast-in-place piers and drilled piers as noted by Dyson

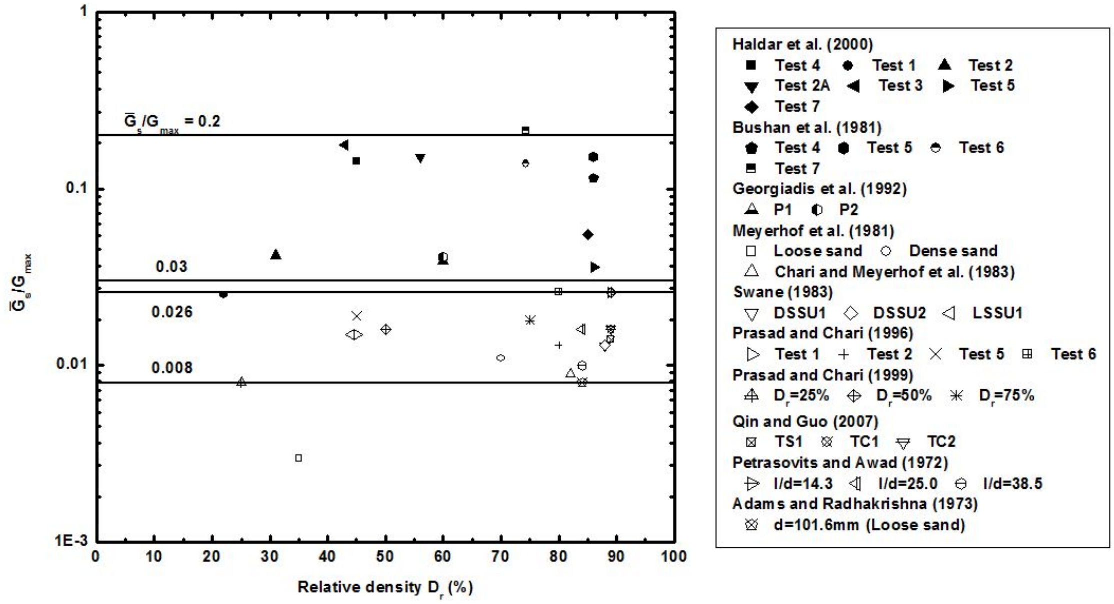


Fig. 12 $\bar{G}_s / G_{max} \sim D_r$ relationship

and Randolph (2001) and Kim *et al.* (2004).

The current correlation of $G_{max}$ with relative densityis less accurate than that with void ratio (Wichtmann and Triantafyllidis 2009). Nevertheless, it is sufficiently accurate for practical purpose.

### 4.4 Estimation of $N_g$

The value of the dimensionless parameter $N_g$ was calculated from the deduced $A_r$ for each test using Eq. (4) and is presented in Table 3.The comparative study shows:

Excluding the five pile tests of F2 (in very loose sand), F6 (in dense crushed stone) and F14-F16 (in clayey sand), the $N_g$ is obtained as 1.0-3.0 (with an average of 1.41) for the 11 full-scale field tests and the three centrifuge tests C1, C2 and C3. This average $N_g$ is 41% higher than that obtained from Eq. (4) with $N_g$ = 1. The current value is consistent with that obtained for 20 flexible piles in sand (Guo and Zhu 2010, Guo 2013a). The latter shows $N_g$ = 0.4-2.8 (with an average of 1.29) but for $p_u$ varying with $z^{1.7}$ owing to the pile flexibility. The value of $N_g$ varies from 0.70 to 4.77 (an average of 2.0) for the 23 model tests.

The $N_g$ decreases with increase in pile diameter or width $d$. In particular, $N_g$ reduces from 0.63 to 0.44 as the width of the rectangular pier increases from 1 m (test C4) to 6 m (test C8). The large pier behaves more as a rigid wall than a pile.

Excluding the three tests F14, F15, and F16 in clayey sand, the back-calculated $N_g$ from the 48 tests in sand and crushed stones were plotted against the normalised pile diameter $d/d_{ref}$ ($d_{ref}$ = 1.0 m) in Fig. 13. The $N_g$ may be correlated with diameter by

$$N_g = (0.4 - 1.8)(d / d_{ref})^{-0.25} \tag{7}$$

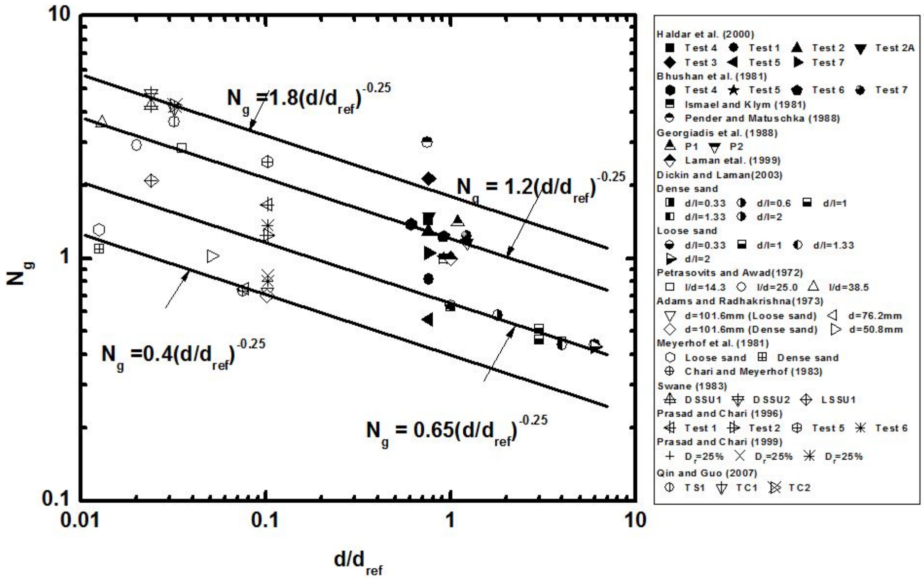


Fig. 13 $N_g - d/d_{ref}$ relationship

## 5. Conclusions

The measured responses of 51 laterally loaded rigid piles in sand have been studied using the elastic-plastic solutions by Guo (2008). The analysis provides the critical parameters $A_r$, $k$ and $k_0$ for the limiting force profile and modulus of subgrade reaction. These results are useful in conducting nonlinear design of lateral piles. The study shows:

(1) The elastic-plastic solution based on a constant $k$ and a linear limiting force profile generally gives good estimation against measured nonlinear response rather than that with a Gibson $k$. Generally, the solution with a constant $k$ should be used to design the lateral piles.

(2) The normalised load capacity reduces while the normalised moment capacity increases, as the ratio $e/l$ increases.

(3) The ratio of $kd/\overline{G}_s$ is 3.27 - 6.91 (with an average of 5.0) for the 16 full-scale field tests and 2 centrifuge tests; and it is 2.37- 5.12 (with an average of 3.7) for the 23 laboratory model tests.

(4) The ratio of $\overline{G}_s / G_{\max}$ is (3-20)% for the 11 full-scale and 2 centrifuge tests and (0.8-2.6)% for 20 model tests, with the $G_{\max}$ being calculated from Eqs. (5)-(6) using the relative density $D_r$. The $\overline{G}_s$ is only a small fraction of the small-strain modulus $G_{max}$.

(5) The $N_g$ may be estimated by $N_g = (0.4 - 1.8)(d/d_{ref})^{-0.25}$. The ultimate pile capacity increases with the increasing $N_g$.

## Acknowledgments

The first author was financially supported by the Endeavour International Postgraduate

Research Scholarship (EIPRS) of Australia and Griffith University Postgraduate Research Scholarship (GUPRS). These supports are gratefully acknowledged.

## References

Adams, J.I. and Radhakrishan, H.S. (1973), “Lateral capacity of deep augured footings”, *Proceedings of the 8th International Conference of Soil Mechanics and Foundation Engineering*, Moscow, Russia, August, Volume 2, pp. 1-8.

Basu, D. and Salgado, R. (2008), “Analysis of laterally loaded piles with rectangular cross sections embedded in layered soil”, *Int. J. Numer. Anal. Meth. Geomech.*, **32**(7), 721-744.

Bhushan, K., Lee, L.J. and Grime, D.B. (1981), “Lateral load tests on drilled piers in sand”, *Proceedings of a Session on Drilled Piers and Caisson, (Sponsored by the Geotechnical Division at the ASCE National Fall Convention)*, St. Louis, MO, USA, October.

Brinch Hansen, J. (1961), “The ultimate resistance of rigid piles against transversal forces”, The Danish Geotechnical Institute, Copenhagen, Denmark, Bulletin No.12, pp. 5-9.

Broms, B.B. (1964), “Lateral resistance of piles in cohesiveless soils”, *J. Soil Mech. Found. Div., ASCE*, **90**(3), 123-156.

Chari, T.R. and Meyerhof, G.G. (1983), “Ultimate capacity of single pile under inclined loads in sand”, *Can. Geotech. J.*, **18**(2), 849-854.

Chen, Y.J., Lin, S.W. and Kulhawy, F.H. (2011), “Evaluation of lateral interpretation criteria for rigid drilled shafts”, *Can. Geotech. J.*, **48**(5), 634-643.

Dickin, E.A. and Laman, M. (2003), “Moment response of short rectangular piers in sand”, *Comput. Struct.*, **81**(30-31), 2717-2729.

Dickin, E.A. and Nazir, R.B. (1999), “Moment-carry capacity of short pile foundations in cohesionless soil”,*J. Geotech.Geoenviron.Eng.*, *ASCE*, **125**(1), 1-10.

Dyson, G.J. and Randolph, M.F. (2001), “Monotonic lateral loading of piles in calcareous sand”, *J. Geotech. Geoenviron. Eng.*, *ASCE*, **127**(4), 346-352.

Fleming, W.G. K., Weltman, A.J., Randolph, M.F. and Elson, W.K. (2009), *Piling Engineering*, Taylor and Francis, London, UK.

Georgiadis, M., Anagnostopoulos, C. and Saflekou, S. (1992), “Centrifuge testing of laterally loaded piles in sand”, *Can. Geotech.J.,* **29**(2), 208-216.

Guo, W.D. (2006), “On limiting force profile, slip depth and response of lateral piles”, *Comput. Geotech.*, **33**(1), 47-67.

Guo, W.D. (2008), “Laterally loaded rigid piles in coheionless soil”, *Can. Geotech. J.*, **45**(5), 676-697.

Guo, W.D. (2012), *Theory and Practice of Pile Foundations*, Spon, London, UK.

Guo, W.D. (2013a), “Simple model for nonlinear response of fifty-two laterally loaded piles”, *J. Geotech. Geoenviron. Eng.*, *ASCE*, **139**(2), 234-252.

Guo, W.D. (2013b), “$P_u$-based solutions for slope stabilizing piles”, *Int. J. Geomech.*, **13**(3), 292-310.

Guo W.D. and Lee, F.H. (2001), “Load transfer approach for laterally loaded piles”, *Int. J. Numer. Anal. Meth. Geomech.*, **25**(11), 1101-1129.

Guo, W.D. and Zhu, B.T. (2010), “Nonlinear response of 20 laterally loaded piles in sand”, *Australian Geomech.*, **45**(2), 67-84.

Haldar, A., Prasad, Y.V.S.N. and Chari, T.R. (2000), “Full-scale field tests on directly embedded steel pole foundations”, *Can. Geotech. J.*, **37**(2), 414-437.

Ismael, N.F. and Klym, T.W. (1981), “Lateral capacity of augered tower foundations in sand”, *IEEE T. Power Ap. Syst.*, **PAS-100**(6), 2963-2968.

Jaky, J. (1944), “The coefficient of earth pressure at rest”, *J. Soc. Hungarian Architect. Eng.* (*Magyar Mernokes Epitesz-Egylet Kozlonye*), 355-358.

Kim, B.T., Kim, N.K., Lee, W.J. and Kim, Y.S. (2004), “Experimental load-transfer curves of laterally loaded piles in Nak-Dong river sand”, *J. Geotech. Geoenviron. Eng.*, *ASCE*, **130**(4), 416-425.

Laman, M., King, G.J.W. and Dickin, E.A. (1999), "Three-dimensional finite element studies of the moment-carrying capacity of short pier foundations in cohesionless soil", *Comput. Geotech.*, **25**(3), 141-155.

Lee, J., Kim, M. and Kyung, D. (2010), "Estimation of lateral load capacity of rigid short piles in sands using CPT results", *J. Geotech. Geoenviron. Eng.*, *ASCE*, **136**(1), 48-56.

Meyerhof, G.G., Mathur, S.K. and Valsangkar, A.J. (1981), "Lateral resistance and deflection of rigid wall and piles in layered soils", *Can. Geotech. J.*, **18**(2), 159-170.

Pender, M.J. and Matuschka, T. (1988), "Interpretation of lateal load tests on rigid poles in cohesionless soils", *Proceedings of the 5th Australia-New Zealand Conference on Geomechanics*, Sydney, Australia, August.

Pestana, J.M. and Salvati, L.A. (2006), "Small-strain behavior of granular soils: Model for cemented and uncemented sands and gravels", *J. Geotech. Geoenviron. Eng.*, *ASCE*, **132**(8), 1071-1081.

Petrasovits, G. and Award, A. (1972), "Ultimate lateral resistance of a rigid pile in cohesionless soil", *Proceedings of the 5th European Conference on Soil Mechanics and Foundation Engineering*, Madrid, Spain, April.

Poulos, H.G. and Davis, E.H. (1980), *Pile Foundation Analysis and Design*, John Wiley and Sons, New York, NY, USA.

Poulos, H.G., Chen, L.T. and Hull, T.S. (1995), "Model tests on single piles subjected to lateral soil movement", *Soils Found.*, **35**(4), 85-92.

Poulos, H.G., Carter, J.P. and Small, J.C. (2001), "Foundations and retaining structures – Research and practice", *Proceedings of the 15th International Conference on Soil Mech. Found. Eng*, Istanbul, Turkey, August.

Prasad, Y.V.S.N. and Chari, T.R. (1996), "Rigid pile with a baseplate under large moments: laboratory model evaluations", *Can. Geotech. J.*, **33**(6), 1021-1026.

Prasad, Y.V.S.N. and Chari, T.R. (1999), "Lateral capacity of model rigid piles in cohesionless soils", *Soils Found.*, **39**(2), 21-29.

Qin, H.Y. (2010), "Response of pile foundations due to lateral force and soil movements", Ph.D. Dissertation, Griffith University, Gold Coast, Australia.

Qin, H.Y. and Guo, W.D. (2007), "An experimental study on cyclic loading of piles in sand", *Proceedings of the 10th Australia New Zealand Conference on Geomech.*, Brisbane, Australia, October.

Scott, R.F. (1981), *Foundation Analysis*, Prentice-Hall, Englewood Cliffs, NJ, USA.

Seed, H.B. and Idriss, I.M. (1970), Soil moduli and damping factors for dynamic response analyses, Report No. EERC 70-10, Earthquake Engineering Research Center, University of California, Berkeley, CA, USA.

Seed, H.B., Wong, R.T., Idriss, I.M. and Tokimatsu, K. (1986), "Moduli and damping factors for dynamic analysis of cohesionless soils", *J. Geotech. Eng.*, *ASCE*, **112**(11), 1016-1032.

Swane, I.C. (1983), "The cyclic behavior of laterally loaded piles", Ph.D. Dissertation, The University of Sydney, Sydney, Australia.

Vucetic, M. and Dobry, R. (1991), "Effect of soil plasticity on cyclic response", *J. Geotech. Eng.*, *ASCE*, **117**(1), 89-107.

Wichtmann, T. and Triantafyllidis, T. (2009), "Influence of the grain-size distribution curve of quartz sand on the small strain shear modulus $G_{max}$", *J. Geotech. Geoenviron. Eng., ASCE*, **135**(10), 1404-1418.

Yan, L. and Byrne, P.M. (1992), "Lateral pile response to monotonic pile head loading", *Can. Geotech. J.*, **29**(6), 955-970.

Zhang, L. (2009), "Nonlinear analysis of laterally loaded rigid piles in cohesionless soil", *Comput. Geotech.*, **36**(5), 718-724.

Zhang, L., Silva, F. and Grismala, R. (2005), "Ultimate lateral resistance to piles in cohesionless soils", *J. Geotech. Geoenviron. Eng.*, *ASCE*, **131**(1), 78-83.

*CC*